

# Jacobian Methods for Dynamic Polarization Control in Optical Applications

Dawei Wang, Kaiqin Lai, Ying Yu, Qi Sui, and Zhaohui Li

**Abstract**—Dynamic polarization control (DPC) is beneficial for many optical applications. It uses adjustable waveplates to perform automatic polarization tracking and manipulation. Efficient algorithms are essential to realizing an endless polarization control process at high speed. However, the standard gradient-based algorithm is not well analyzed. Here we model the DPC with a Jacobian-based control theory framework that finds a lot in common with robot kinematics. We then give a detailed analysis of the condition of the Stokes vector gradient as a Jacobian matrix. We identify the multi-stage DPC as a redundant system enabling control algorithms with null-space operations. An efficient, reset-free algorithm can be found. We anticipate more customized DPC algorithms to follow the same framework in various optical systems.

**Index Terms**—polarization control, signal processing.

## I. INTRODUCTION

**P**OLARIZATION management is an important topic in multiple areas of optics, such as optical sensing [1], optical communication [2], and quantum information [3]. One extensively researched type of the polarization management is called dynamic polarization control (DPC), which played a crucial role in the early development of coherent optical fiber communication [4] and has been successfully utilized in recent studies of self-homodyne coherent optical detection [5] and quantum key distribution [6]. The DPC typically performs transformation from an arbitrary input state of polarization (SOP) to a desired output SOP via in-line control, a useful feature to perform tasks such as polarization alignment, polarization demultiplexing, and polarization stabilization in various optical systems.

Numerous DPC schemes have been proposed and tested, almost all of which can be modeled as a system of waveplates. Fig. 1 shows the picture of a widely used manual fiber polarization controller, which is equivalent to three rotatable waveplates connected in series. Most DPC schemes use

This work was supported in part by the National Key Research and Development Program of China (2019YFB1803502), in part by the National Natural Science Foundation of China (U2001601), and in part by the Key-Area Research and Development Program of Guangdong Province (2018B010114002, 2020B0303040001). (*Corresponding author: Dawei Wang, Kaiqin Lai*)

D. Wang and Z. Li are with Guangdong Provincial Key Laboratory of Optoelectronic Information Processing Chips and Systems, School of Electronics and Information Technology, Sun Yat-sen University, Guangzhou 510006, China, and also with Southern Marine Science and Engineering Guangdong Laboratory (Zhuhai), Zhuhai 519000, China (e-mails: wangdw9@mail.sysu.edu.cn; lzhh88@mail.sysu.edu.cn).

K. Lai and Y. Yu are with Guangdong Provincial Key Laboratory of Optoelectronic Information Processing Chips and Systems, School of Electronics and Information Technology, Sun Yat-sen University, Guangzhou 510006, China (e-mails: laikq5@mail2.sysu.edu.cn).

Q. Sui is with Southern Marine Science and Engineering Guangdong Laboratory (Zhuhai), Zhuhai 519000, China (e-mails: suiqi@sml-zhuhai.cn).

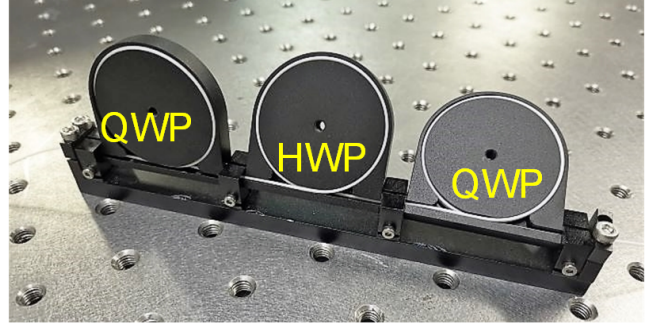


Fig. 1. Manual polarization controller with optical fiber coils working as rotatable waveplates. QWP: quarter-wave plate. HWP: half-wave plate.

similar structure but have different physical realizations of the waveplates and also require additional control circuits. Examples of such schemes include the one based on fiber squeezer [7], liquid crystal, lithium niobite ( $\text{LiNbO}_3$ ) crystal [8], metasurfaces [9], and plasma [10]. Although seemingly different, they can be effectively modeled as waveplates with variable thickness and/or adjustable principal axes [11], [12]. Notably, the rapidly developing photonics integration provides both ideas and techniques for realizing smaller and faster polarization controllers. Several platforms on which integrated polarization control devices with impressive performance have been reported [13], [14], [15], [16].

The DPC tracking speed is of primary concern among several parameters. It relies on the optical components with fast response to external control electronics and control algorithms with low latency. Fast polarization response (on the order of  $10^5$  rad/s) can be realized via, e.g., the Pockels effect of  $\text{LiNbO}_3$  crystals. A well-designed DPC algorithm should be able to track the input SOP, which may vary randomly and indefinitely, with control signals of a limited range. Control signal reset near the range limit is nonetheless allowed, provided that the output SOP does not change during the reset process. The most widely used gradient descent algorithm uses a dithering technique to estimate the current SOP gradient (with respect to the control signal) with sophisticated signal-reset strategies [4]. The dithering is simple to implement but would inevitably suspend the control loop repeatedly. The signal reset is particular to the type of DPC component and adds considerable complexity to programming. Other control algorithms also exist, such as greedy linear descent [17], genetic algorithm [18] and particle swarm optimization algorithm [19], but they are considerably more complex than the gradient-based one.

The DPC is a typical system that fits the Jacobian-based control theory framework, known as the Resolved Motion Rate Control in robotics [20][21, chap. 8]. When the control targets (such as the position of controlled object) are viewed as a vector-valued function of several free variables (force, voltage, temperature, etc.), the Jacobian is the matrix of all its first-order partial derivatives which is useful for linearizing the control problem. In the DPC problem, the target Stokes vector as a function of the free parameters of a multi-stage DPC device can also be linearized via the Jacobian. However, there still lacks detailed analyses of the Jacobian condition for a general DPC model in the literature. In contrast, this is a well-studied topic in robotics [22]. We find that many control techniques that have been widely used in robotics can be analogously designed and applied to the DPC problem despite distinct application scenarios and requirements. In this article, we give a detailed analysis of the Jacobian condition based on a generalized DPC model. We further introduce and study several standard Jacobian-based control methods for the polarization control applications. We successfully prove that the Jacobian of a general multi-stage DPC device is almost always rank deficient. We also find that the gradient projection method enables reset-free endless polarization control by taking advantage of the null space of an underdetermined DPC Jacobian. In view of its generality, we anticipate more variants of DPC algorithms with distinct features in the same theoretical framework.

## II. THE DPC PROBLEM

In the classical regime, a fully polarized light is in a definite polarization state that can be described by a real-valued Stokes vector  $S = [s_1, s_2, s_3]^T$  with  $T$  for transpose and the property  $s_1^2 + s_2^2 + s_3^2 = 1$ . Therefore, all possible polarization states can be represented uniquely as a point on a sphere, namely the Poincaré sphere. The transformation between the input states  $S_{in}$  and the output state  $S_{out}$  of a polarization control element (i.e., a general waveplate) is then equivalent to the 3-dimensional rotation,  $S_{out} = MS_{in}$ , where the rotation matrix  $M$ , known as the Mueller matrix, is an orthogonal matrix if the polarization control is lossless. As examples, when the three orthogonal axial vectors  $S_1 = [1, 0, 0]^T$ ,  $S_2 = [0, 1, 0]^T$ , and  $S_3 = [0, 0, 1]^T$  form a right-handed coordinate system, the waveplates that rotate  $S_{in}$  by an angle  $\theta$  about  $S_1$ ,  $S_2$  and  $S_3$  are described respectively by the elemental rotation matrices

$$R_1 = \begin{bmatrix} 1 & 0 & 0 \\ 0 & \cos(\theta) & -\sin(\theta) \\ 0 & \sin(\theta) & \cos(\theta) \end{bmatrix} \quad R_2 = \begin{bmatrix} \cos(\theta) & 0 & \sin(\theta) \\ 0 & 1 & 0 \\ -\sin(\theta) & 0 & \cos(\theta) \end{bmatrix}$$

and

$$R_3 = \begin{bmatrix} \cos(\theta) & -\sin(\theta) & 0 \\ \sin(\theta) & \cos(\theta) & 0 \\ 0 & 0 & 1 \end{bmatrix}.$$

The rotation direction follows the right-hand rule such that the axial vector coincides with the angular velocity vector. A general representation of 3d rotation matrix is given by

$$M = I + [\sin(\theta)](\vec{r} \times) + [1 - \cos(\theta)](\vec{r} \times)^2 \quad (1)$$

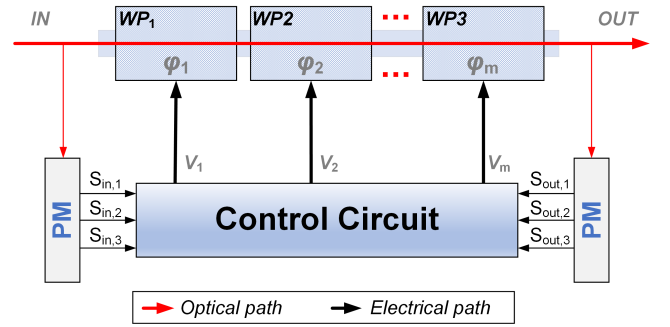


Fig. 2. Block diagram of the dynamic polarization control system with serial-linked waveplates and Jacobian-based control loops. The waveplates have key parameters  $\varphi_{1,2,\dots}$  for altering the SOP at the output.  $V_{1,2,\dots}$  are the control voltages produced by the control circuit. Small portions of light are decoupled from both the input and the output for Stokes parameters measurement. WP: waveplate. PM: polarimeter.

where  $\vec{r}$  is the unit axial vector and  $\vec{r} \times$  is the cross product matrix of  $\vec{r}$ . Note that all the entries of matrix  $M$  are real-valued.

To convert an arbitrary  $S_{in}$  into a designated  $S_{out}$  means the polarization controller needs to be reconfigurable for realizing all possible Mueller matrices. In practice, this is achieved via composition, i.e., a system consists of multiple serial-linked polarization control components having different characteristic rotation matrices. As a result, the  $m$ -stage DPC is modeled as a sequence of non-commutative polarization rotations, i.e.,  $S_{out} = M_m M_{m-1} \cdots M_1 S_{in}$ , which represents a trajectory connecting the input and output SOP points on the Poincaré sphere. A common rule for the composition is *Euler angles*. E.g., an arbitrary 3d rotation can be written as a combination of three elemental rotations  $M = R_1(\theta_3)R_3(\theta_2)R_1(\theta_1)$  where  $\theta_1$ ,  $\theta_2$ , and  $\theta_3$  are three angles to be determined by the control logic. The reverse process of finding the three angles suffers from nonuniqueness and singularities in the motion of a rigid body, which uses intrinsic rotations such as the roll-pitch-yaw angles. However, the DPC stages have independent axes and hence deal with *extrinsic rotations* in the world coordinate frame. I.e., one should picture the DPC process as a series of rotations of the Poincaré sphere.

Note that although each  $M$  can have multiple parameters that we can control, the Euler-angles composition uses one control variable for each DPC stage, which is very common in practical design due to easy implementation. The DPC of this type needs at least 3 stages (3 degrees of freedom (DOF)) to specify an arbitrary 3d rotation. But the SOP points on the Poincaré sphere have only two DOFs, i.e. the longitude and latitude, or the azimuth and ellipticity<sup>1</sup>. We say that the DPC with three or more stages is inherently redundant because it can realize infinitely many rotations (one is *geodesic*) that connect a given pair of SOP points on the Poincaré sphere.

To formalize the DPC problem, consider an  $m$ -stage DPC with voltage-driven constituent waveplates modeled as Mueller matrices  $M_1, \dots, M_m$ , which are parameterized with scalar

<sup>1</sup>Imagine the Stokes vector as an airplane located at the origin of Poincaré sphere pointing outwards. the DPC is similar to the aircraft attitude control but simpler because the Stokes vector has no meaningful *roll* motion.

external control signals  $\varphi_1, \dots, \varphi_m$ , respectively. Define the vector  $\varphi \equiv [\varphi_1, \dots, \varphi_m]^T$ . The critical step is to model the DPC process as the transformation from the  $m$ -dimensional  $\varphi$ -space to the 3-dimensional Stokes space. Namely,

$$S_{\text{out}} = \underbrace{M_m(\varphi_m)M_{m-1}(\varphi_{m-1}) \cdots M_1(\varphi_1)}_{f(\varphi)} S_{\text{in}}, \quad (2)$$

where the Stokes vector is arguably the best choice to represent the 2-DOF control task for practical reasons of easy measurement. Other representation such as the longitude and latitude may not be well defined at certain locations in the task space (e.g., two poles of the Poincaré sphere).

In general, the mapping  $f : \varphi \rightarrow S_{\text{out}}$  is nonlinear and determined by definition by both the input SOP and the constituent Mueller matrix. The DPC problem seeks a solution by reconfiguring all the waveplates via adjusting  $\varphi$  to reach the target  $S_{\text{out}}$  with varying  $S_{\text{in}}$ , subject to the condition that each of  $\varphi_i$ ,  $i = 1, \dots, m$ , is limited to a finite range. It is often the case that  $\varphi_i$  is linearly related to the rotation angle about a fixed axis in the  $i$ th stage. We can also realize adjustable axis by combining several fixed-axis stages. E.g., the combination  $R_3(\phi)R_1(\theta)R_3^T(\phi)$  represents the rotation of angle  $\theta$  around an  $\phi$ -oriented axis in the  $S_1$ - $S_2$  plane. Care must be taken to obtain an accurate model especially when the voltages are nonlinearly related to the adjustable axes.

The DPC problem formulated above closely resembles the arm-type robot kinematics, where the  $S_{\text{out}}$  can be considered as the state of the robot end-effector, and the  $m$  waveplates are the  $m$  serial-linked robot arms [21]. Both waveplates and robot arms have physical limitations in their maximal tuning ranges. Given  $S_{\text{in}}$  and  $\varphi$ , the output state  $S_{\text{out}}$  can be computed via (2), which is termed *forward* kinematics in robotics (the mapping from robot configuration to end-effector pose, see [21, sec. 7.1]). Finding the required control signals for realizing a specific  $S_{\text{out}}$  corresponds to the *inverse* kinematics problem in robotics (the inverse mapping of forward kinematics, see [21, sec. 7.2]). The two problems (DPC vs. robotics) differ in the dimensionality of their task spaces (2 DOF in DPC vs. 6 DOF in most robotics).

It is in general difficult to solve for  $\varphi$  by direct inversion of the mapping  $f$ . Also, the redundant DPC means we may find infinite solutions for a given SOP target. However, the model can be *linearized* when small variations  $\Delta\varphi$  in the control signals are considered, in which cases the model (2) becomes

$$J\Delta\varphi = \Delta S_{\text{out}}, \quad (3)$$

where  $J$  is the  $3 \times m$  Jacobian matrix defined as  $J = \partial f / \partial \varphi$  evaluated at the point of linearization, i.e.,

$$J = \begin{bmatrix} \frac{\partial s_{1,\text{out}}}{\partial \varphi_1} & \frac{\partial s_{1,\text{out}}}{\partial \varphi_2} & \cdots & \frac{\partial s_{1,\text{out}}}{\partial \varphi_m} \\ \frac{\partial s_{2,\text{out}}}{\partial \varphi_1} & \frac{\partial s_{2,\text{out}}}{\partial \varphi_2} & \cdots & \frac{\partial s_{2,\text{out}}}{\partial \varphi_m} \\ \frac{\partial s_{3,\text{out}}}{\partial \varphi_1} & \frac{\partial s_{3,\text{out}}}{\partial \varphi_2} & \cdots & \frac{\partial s_{3,\text{out}}}{\partial \varphi_m} \end{bmatrix}, \quad (4)$$

$\Delta\varphi$  and  $\Delta S_{\text{out}}$  are implicitly the rates of coordinate change in  $\varphi$ -space and Stokes space respectively, as they are variations over a small amount of time (consider dividing both sides of (3) by  $\Delta t$ ).

To form a closed-loop control,  $\Delta S_{\text{out}}$  is taken to be the error between the current and the target SOP, i.e.,

$$\Delta S_{\text{out}}[k] = S_{\text{out}}^* - S_{\text{out}}[k], \quad (5)$$

where  $S_{\text{out}}[k]$  is the measured Stokes vector at time instance  $k$ . Then, the optimal  $\Delta\varphi$  can be found based on the linear model (3) with methods we shall introduce in the next section. The waveplates are driven by the updated signal

$$\varphi[k+1] = \varphi[k] + \Delta\varphi[k]. \quad (6)$$

The schematic of the Jacobian-based DPC is depicted in Fig. 2. Light is partially decoupled from both the input and the output optical paths to measure the current  $S_{\text{in}}$  and  $S_{\text{out}}$ . A polarization measuring device based on photonics integration can be found in [15]. This is however optional at the output as it is possible to directly compute  $S_{\text{out}}$  from (2). The control circuit computes the Jacobian, solves the control model (3) to obtain the best  $\Delta\varphi$ , and drives the waveplates with updated voltages. Since knowing the waveplate matrices and  $S_{\text{in}}$  determines the Jacobian completely, no dithering is needed if the closed-form Jacobian can be obtained.

### III. JACOBIAN METHODS

#### A. Direct or pseudo inversion

The condition of the Jacobian matrix is critical for solving the linear model (3). A 3-stage DPC has a  $3 \times 3$  square Jacobian matrix. If the matrix is invertible, the control signals variation can be found easily via  $\Delta\varphi = J^{-1}\Delta S_{\text{out}}$ , where  $(\cdot)^{-1}$  stands for matrix inverse and  $\Delta S_{\text{out}}$  is given by (5). Consider  $\varphi$  as voltages that produce linearly-related rotation angles only. It turns out that all 3-stage DPC modeled by (2) has noninvertible Jacobian of the form

$$J = [M_3 M_2 (\vec{r}_1 \times S') \quad M_3 (\vec{r}_2 \times S'') \quad \vec{r}_3 \times S'''] , \quad (7)$$

where  $\vec{r}_{1,2,3}$  are the rotation axes of Mueller matrices  $M_{1,2,3}$ , respectively, whereas  $S'$ ,  $S''$ , and  $S''' = S_{\text{out}}$  are the Stokes vectors out of the first, the second, and the third stage of DPC, respectively. The rank of Jacobian is  $\leq 2$  regardless of the input SOP or the DPC configurations since all the column vectors of  $J$  are perpendicular to  $S_{\text{out}}$ . The singularity is explicit whenever  $S'$ ,  $S''$ , or  $S'''$  coincides with the rotation axis of the corresponding stage, which has consequences in the DPC performance (see next section). The results hold when  $\varphi_i$  is an arbitrary (linear or nonlinear) function of the corresponding rotation angle. Moreover, by using the concept of polarization dynamic eigenstates [23], the results can be generalized to the cases where  $\varphi$  is related to any type of control parameters that causes SOP changes at the DPC output. The form of (7) is a general result since the dynamic eigenstate  $\vec{r}$  of matrix  $M$  follows the rule [23, equ. 14]

$$\frac{dM}{d\varphi} = \vec{r} \times M, \quad (8)$$

where  $\varphi$  is the key parameter causing the SOP change.

To get around the singularity problem, we can use alternative methods to find  $\Delta\varphi$ , such as the transposed Jacobian,

$\Delta\varphi = J^T \Delta S_{\text{out}}$  with  $(\cdot)^T$  for transpose, the damped Jacobian,  $\Delta\varphi = (J + \lambda I)^{-1} \Delta S_{\text{out}}$  where  $\lambda$  is a proper constant and  $I$  the identity matrix, or the pseudo inverse Jacobian  $\Delta\varphi = J^+ \Delta S_{\text{out}}$  with  $(\cdot)^+$  for the Moore-Penrose inverse. The pseudo inverse solution has the feature of being minimum norm among all viable solutions.

The square  $J$  being singular means the linear model (3) is underdetermined (or *overactuated* in robotics) for all  $m \geq 3$  to which the pseudo inverse method is applicable. Moreover, it is easy to verify that the rank of Jacobian is  $\leq 2$  for all  $m > 3$  due to the same reasons for (7), even when the DPC has many stages. It implies immediately that the matrix  $JJ^T$  is noninvertible but the MP inverse of  $J$  can only be evaluated via, e.g. the singular value decomposition (SVD)<sup>2</sup>. The manipulability index  $m = \sqrt{\det(JJ^T)}$  is also zero. The fact we have a Jacobian with only 2 degrees-of-freedom regardless of the number of DPC stages is in sharp contrast to the classical kinematics problem.

### B. Gradient projection method

The underdetermined  $m$ -stage DPC modeled by (3) means there is no unique solution for  $\Delta\varphi$ . But all feasible solutions differ by a vector in the null space of  $J$ , i.e.,  $\Delta\varphi = \Delta\varphi_0 - N\delta$ , where  $\Delta\varphi_0$  is an initial solution, the columns of  $N$  are the null-space basis vectors of  $J$ , and  $\delta$  is an arbitrary vector. Therefore, It is possible to impose further constraints on  $\varphi$  when searching for the optimal  $\Delta\varphi$  by exploiting this degree of freedom in the null space. The *gradient projection method* chooses a particular  $N\delta$  as the projection of  $\varphi$  onto the null space of  $J$  to minimize the norm of  $\varphi$ . Namely,

$$\Delta\varphi = J^+ \Delta S_{\text{out}} - NN^+ \varphi \quad (9)$$

$$= J^+ \Delta S_{\text{out}} - (I - J^+ J) \varphi, \quad (10)$$

where  $\Delta S_{\text{out}}$  is again defined by (5). Note that there is no need to actually compute the matrix  $N$  by using (10), which constitutes the initial solution  $\Delta\varphi_0 = J^+ \Delta S_{\text{out}}$  and the null-space term  $\Delta\varphi_1 = (I - J^+ J) \varphi$ . Since the linear model is assumed for a local space, which may not contain the actual minimum  $\varphi$ , one may take a small step towards  $\Delta\varphi_1$  such that  $\Delta\varphi = \Delta\varphi_0 + \mu \Delta\varphi_1$  converges to the globally optimal  $\varphi$  with  $0 < \mu < 1$ . The classical way to reset the control signals without changing the polarization state [4] is similar to null-space operation discussed here. However, it is a complicated task to find such reset strategies when working with the nonlinear mapping given by (2).

### C. Extended Jacobian method

The gradient projection method can be viewed as the solution to minimize the cost function  $H = \|\varphi\|^2$  subject to the equality constraint given by (2). At the point of  $H$  reaching its minimum for the underdetermined system,  $H$  should not change over small variations in the null space of system Jacobian. Namely, the projection of the gradient of  $H$  onto

<sup>2</sup>There are methods to address the singular  $JJ^T$  explicitly, such as the regularized least squares  $\Delta\varphi = J^T (JJ^T + \lambda I)^{-1} \Delta S_{\text{out}}$  which minimizes the sum  $\|J\Delta\varphi - \Delta S_{\text{out}}\|^2 + \|\Delta\varphi\|^2$ .

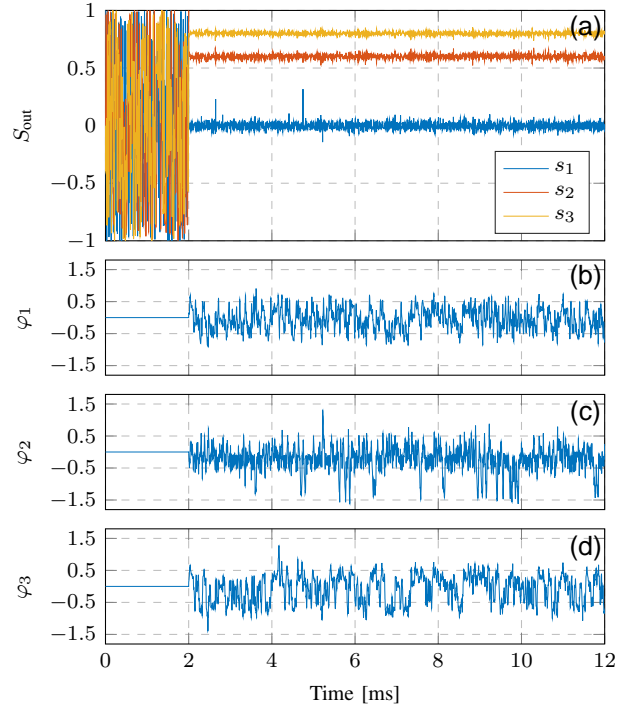


Fig. 3. Simulation results of using a 3-stage DPC for locking the scrambled input SOP to the designated output SOP at  $[0, 0.6, 0.8]^T$ . (a) The time evolution of the Stokes parameters at the output (DPC activated after 2 ms). (b-d) The control signal for each stage.

the null space is zero. Therefore, at those points, the system satisfies the following equations [24], with dot operation for inner product,

$$\begin{bmatrix} f(\varphi) \\ N(\varphi) \cdot \frac{\partial H}{\partial \varphi} \end{bmatrix} = \begin{bmatrix} S_{\text{out}} \\ \mathbf{0} \end{bmatrix}, \quad (11)$$

which can be linearized at  $\varphi_o$  as

$$\underbrace{\begin{bmatrix} J \\ \frac{\partial}{\partial \varphi} [N(\varphi) \cdot \frac{\partial H}{\partial \varphi}] \end{bmatrix}}_{J_e} \Delta\varphi = \begin{bmatrix} \Delta S_{\text{out}} \\ -N(\varphi_o) \cdot \frac{\partial H}{\partial \varphi_o} \end{bmatrix}. \quad (12)$$

We obtain a square matrix, called the extended Jacobian  $J_e$ , on the left hand side when  $J$  is of full rank. The solution of these equations are found by taking the direct inversion of  $J_e$  if it is nonsingular.

Note that  $\partial H / \partial \varphi$  is simply the  $\varphi$  vector for  $H = \|\varphi\|^2$ , which means the desired  $\varphi$  should be orthogonal to the null space of  $J$  according to the formulation in (11). When we ignore the second-order term  $\partial N(\varphi) / \partial \varphi$ , (12) reduces to

$$\begin{bmatrix} J \\ N^T \end{bmatrix} \Delta\varphi = \begin{bmatrix} \Delta S_{\text{out}} \\ -N(\varphi_o) \cdot \varphi_o \end{bmatrix}. \quad (13)$$

A simple method to compute the null-space basis vector  $N$  for a 4-stage DPC is given by [24]

$$N = [\Delta_1, \Delta_2, \Delta_3, \Delta_4] \\ \Delta_i = (-1)^{i+1} \det(J^1, J^2, \dots, J^{i-1}, J^{i+1}, \dots, J^4), \quad (14)$$

where  $\det(\cdot)$  is the determinant with  $J^i$  the  $i$ th column of  $J$ . However, the standard extended Jacobian cannot be used for



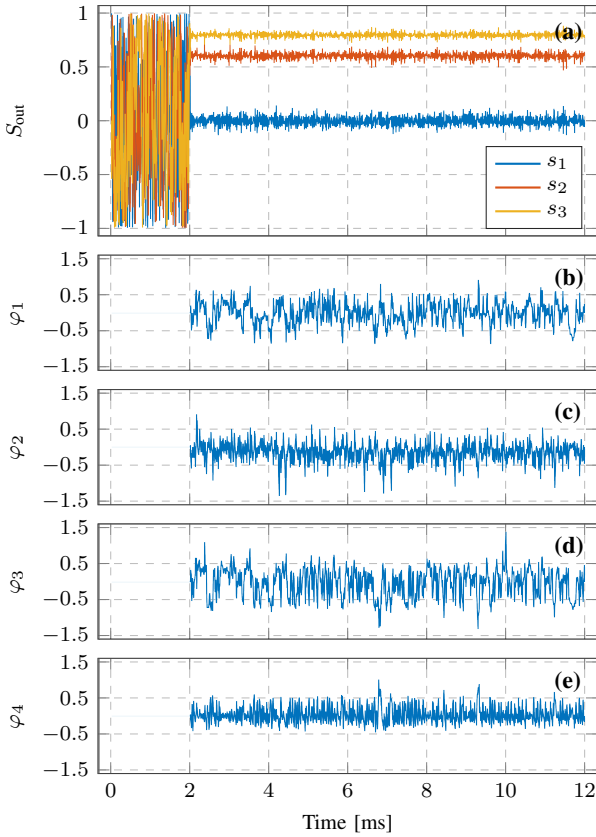


Fig. 4. Simulation results of using a 4-stage DPC for locking the scrambled input SOP to the designated output SOP at  $[0, 0.6, 0.8]^T$ . (a) The time evolution of the Stokes parameters at the output (DPC activated after 2 ms). (b-e) The control signal for each stage.

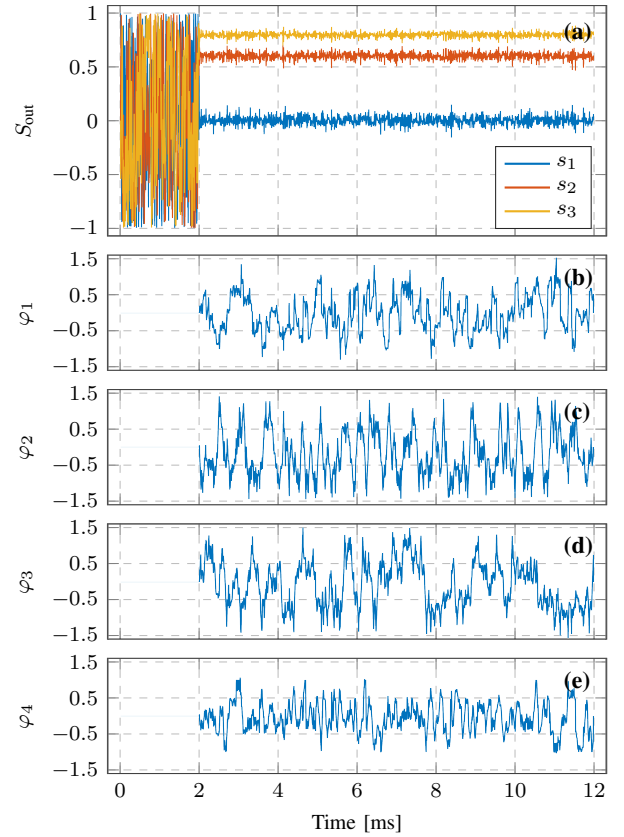


Fig. 5. Simulation results of using a 4-stage DPC for locking the scrambled input SOP to the designated output SOP at  $[0, 0.6, 0.8]^T$ . The gradient projection is only included when the controls signals exceed a threshold. (a-e) The same plotting as that in Fig. 4.

the DPC model when  $J$  is not full rank, which leads to a singular  $J_e$  in (12) and (13).

#### D. Special cases

The analysis we have given so far is fully general whereas special cases exist in real applications. For instances, the desired SOP target may not be a single point on the Poincaré sphere but a particular region, say, all points with  $s_3 = 0$ . In such cases, the linear DPC model has an output space with one dimension and an  $1 \times m$  Jacobian. The gradient projection method is applicable and, since  $J$  now has full rank, we should be able to find  $m - 1$  basis vectors in its null space and get an invertible extended Jacobian.

## IV. RESULTS AND DISCUSSION

We conduct numerical simulations by sending a polarization scrambled light into the DPC with Euler-angles composition. The input SOP is characterized by the rotation about the axis  $S_3$  with a constant rate of 100 krad/s, perturbed by the rotation about the axis  $S_2$  with randomly distributed angles. The acquisition rate of  $S_{\text{out}}$  is set to be 50 MHz and the DPC is activated after 2 ms. The overall processing delay  $\tau$  of the closed-loop DPC is assumed to be  $10^{-6}$  second, meaning that the  $\Delta\varphi$  obtained at time  $t$  is used to update the control signal at  $t + \tau$ .

First, we study a 3-stage DPC system with the composition given by  $M = R_1 R_3 R_1$  and the 3 control signals are linearly related to the rotation angles via  $\theta = \pi \cdot \varphi$ , i.e., one unit of control signal generates  $\pi$  phase shift. The target SOP is  $[0, 0.6, 0.8]^T$ . The gradient projection method is used to obtain the phase variations with a step size of 0.1. The time evolution of the individual entries of the vector  $S_{\text{out}}$  is shown in Fig. 3(a), showing successful SOP convergence is rapidly achieved when the DPC is activated after 2 ms. The required control signals, as shown in Fig. 3(c), are clearly well bounded (mostly  $\in (-1.5, 1.5)$ ). The target SOP is chosen for better illustration only. However, we do observe that the control signals have more outliers with large values when the  $S_{\text{out}}^*$  coincides with the rotation axis of the last stage, which zeros the last column of Jacobian such that it is more likely to have a small second singular value after the SVD. The outliers also represent the situations when the DPC is close to loss another DOF and become a 1-rank system.

The control performance can be improved by using a 4-stage DPC. The results based on the composition  $M = R_1 R_3 R_1 R_3$  and the same settings as above are shown in Fig. 4. We obtain now a better SOP convergence and control phases varying over a slightly smaller range.

The computational complexity of the gradient projection method lies in the computation of Jacobian matrix, the SVD-based pseudo inverse and the null space correction term. In

the examples we present here, the Jacobian has a relatively simple form but does need real-time update since it depends on the varying input SOP explicitly. The pseudo inverse seems inevitable and requires efficient algorithm to implement. On the other hand, we need not to include the null space term all the time unless the control signals are close to their boundaries. We study the case by only activating the null-space correction when one of the control signals exceeding  $\pm 1$ . The results are shown in Fig. 5. To compare with the results in Fig. 4, it turns out the null-space correction needs only to be included about 20% of the operation time without sacrificing the DPC performance. The percentage clearly depends on the SOP varying speed at the DPC input. We note that the gradient projection can be activated much like the classical signal resetting, but in a more systematic way.

The Euler-angles composition is obviously just one of many possible DPC realizations. For other DPC solutions, it might be difficult, if not impossible, to get a close-form Jacobian so that techniques like dithering becomes essential. As results, the Jacobian condition may not be as clear as the examples shown in this article. However, the gradient projection method applies to any type of DPC as long as it can be modeled by an underdetermined linear model. The extended Jacobian method, on the other hand, asks for a Jacobian matrix with full rank.

## V. CONCLUSION

We have discussed several Jacobian-based algorithms for fast and reset-free dynamic polarization control (DPC). By linearizing the general mapping from the control space to the Stokes space, we have shown that the DPC problem can be linked closely to the arm-type robot kinematics. Methods including the gradient projection and the extended Jacobian are analyzed based on a popular DPC realization. We have analyzed in detail on the Jacobian condition of the DPC modeled as multiple series-lined waveplates with Euler-angles composition. We confirm the Jacobian has rank deficiency when the number of waveplates is larger than or equal to 3. Numerical simulations of gradient projection demonstrate the usage of null-space correction for confining the physical range of control signal. The results of this work can be generalized for other DPC models, the Jacobian condition of which however demands a case-by-case analysis.

## REFERENCES

- [1] C. Caucheteur, T. Guo, and J. Albert, "Polarization-assisted fiber bragg grating sensors: Tutorial and review," *Journal of Lightwave Technology*, vol. 35, no. 16, pp. 3311–3322, 2017.
- [2] M. Martinelli, P. Martelli, and S. M. Pietralunga, "Polarization stabilization in optical communications systems," *Journal of Lightwave Technology*, vol. 24, no. 11, pp. 4172–4183, 2006.
- [3] X.-S. Ma, T. Herbst, T. Scheidl, D. Wang, S. Kropatschek, W. Naylor, B. Wittmann, A. Mech, J. Kofler, E. Anisimova *et al.*, "Quantum teleportation over 143 kilometres using active feed-forward," *Nature*, vol. 489, no. 7415, pp. 269–273, 2012.
- [5] T. Gui, X. Wang, M. Tang, Y. Yu, Y. Lu, and L. Li, "Real-time demonstration of homodyne coherent bidirectional transmission for next-generation data center interconnects," *Journal of Lightwave Technology*, vol. 39, no. 4, pp. 1231–1238, 2021.
- [4] R. Noe, H. Heidrich, and D. Hoffmann, "Endless polarization control systems for coherent optics," *Journal of Lightwave Technology*, vol. 6, no. 7, pp. 1199–1208, 1988.
- [6] P. Jouguet, S. Kunz-Jacques, A. Leverrier, P. Grangier, and E. Diamanti, "Experimental demonstration of long-distance continuous-variable quantum key distribution," *Nature Photonics*, vol. 7, no. 5, pp. 378–381, 2013.
- [7] W. H. Aarts and G.-D. Khoe, "New endless polarization control method using three fiber squeezers," *Journal of Lightwave Technology*, vol. 7, no. 7, pp. 1033–1043, 1989.
- [8] R. Noé, B. Koch, and V. Mirvoda, "LiNbO<sub>3</sub>-based endless optical polarization control," in *2016 21st European Conference on Networks and Optical Communications (ECOC)*. IEEE, 2016, pp. 162–167.
- [9] J. Park, J.-H. Kang, S. J. Kim, X. Liu, and M. L. Brongersma, "Dynamic reflection phase and polarization control in metasurfaces," *Nano Letters*, vol. 17, no. 1, pp. 407–413, 2017.
- [10] D. Turnbull, P. Michel, T. Chapman, E. Tubman, B. Pollock, C. Chen, C. Goyon, J. Ross, L. Divol, N. Woolsey *et al.*, "High power dynamic polarization control using plasma photonics," *Physical Review Letters*, vol. 116, no. 20, p. 205001, 2016.
- [11] K. Hirabayashi and C. Amano, "Feed-forward continuous and complete polarization control with a PLZT rotatable-variable waveplate and inline polarimeter," *Journal of Lightwave Technology*, vol. 21, no. 9, pp. 1920–1932, 2003.
- [12] A. J. van Haasteren, J. J. van der Tol, M. O. Van Deventer, and H. J. Frankena, "Modeling and characterization of an electrooptic polarization controller on LiNbO<sub>3</sub>," *Journal of Lightwave Technology*, vol. 11, no. 7, pp. 1151–1157, 1993.
- [13] J. Sarmiento-Merenguel, R. Halir, X. Le Roux, C. Alonso-Ramos, L. Vivien, P. Cheben, E. Durán-Valdeiglesias, I. Molina-Fernández, D. Marris-Morini, D.-X. Xu *et al.*, "Demonstration of integrated polarization control with a 40 dB range in extinction ratio," *Optica*, vol. 2, no. 12, pp. 1019–1023, 2015.
- [14] X. Wang, Y. Zeng, R. Liao, C. Zhao, H. Wu, and M. Tang, "Mach-Zehnder interferometer based endlessly adaptive polarization controller on silicon-photon platform," in *2021 Optical Fiber Communications Conference and Exhibition (OFC)*. IEEE, 2021, pp. 1–3.
- [15] Z. Lin, Y. Lin, H. Li, M. Xu, M. He, W. Ke, H. Tan, Y. Han, Z. Li, D. Wang, X. S. Yao, S. Fu, S. Yu, and X. Cai, "High-performance polarization management devices based on thin-film lithium niobate," *Light: Science & Applications*, vol. 11, no. 93, pp. 1–9, 2022.
- [16] W. Liu, J. Liao, H. Cai, Y. Yu, and X. Zhang, "High-speed silicon integrated polarization stabilizer assisted by a polarimeter," *Journal of Lightwave Technology*, vol. 40, no. 12, pp. 3794–3801, 2022.
- [17] M. Ma, H. Shoman, K. Tang, S. Shekhar, N. A. Jaeger, and L. Chrostowski, "Automated control algorithms for silicon photonic polarization receiver," *Optics Express*, vol. 28, no. 2, pp. 1885–1896, 2020.
- [18] G. Mamdoohi, A. F. Abas, K. Samsudin, N. H. Ibrahim, A. Hidayat, and M. A. Mahdi, "Implementation of genetic algorithm in an embedded microcontroller-based polarization control system," *Engineering Applications of Artificial Intelligence*, vol. 25, no. 4, pp. 869–873, 2012.
- [19] Q. Chen, T. Liu, K. Liu, J. Jiang, Z. Ding, L. Zhang, Y. Li, L. Pan, and C. Ma, "An elimination method of polarization-induced phase shift and fading in dual Mach-Zehnder interferometry disturbance sensing system," *Journal of Lightwave Technology*, vol. 31, no. 19, pp. 3135–3141, 2013.
- [20] D. E. Whitney, "Resolved motion rate control of manipulators and human prostheses," *IEEE Transactions on Man-Machine Systems*, vol. 10, no. 2, pp. 47–53, 1969.
- [21] P. Corke, *Robotics, Vision and Control: Fundamental algorithms in MATLAB® second edition*. Springer, 2017.
- [22] B. Siciliano, "Kinematic control of redundant robot manipulators: A tutorial," *Journal of Intelligent and Robotic Systems*, vol. 3, no. 3, pp. 201–212, 1990.
- [23] W. Shieh and H. Kogelnik, "Dynamic eigenstates of polarization," *IEEE Photonics Technology Letters*, vol. 13, no. 1, pp. 40–42, 2001.
- [24] P. H. Chang, "A closed-form solution for inverse kinematics of robot manipulators with redundancy," *IEEE Journal of Robotics and Automation*, vol. RA-3, no. 5, pp. 393–403, 1987.